TITLE: Endosomal sorting protein SNX4 limits synaptic vesicle docking and release

Authors: Poppinga, J [1]*, Barret, N.J. [1], Cornelisse, L.N. [1,2], Verhage, M.[1,2], van Weering, J.R.T. [1,2#]
[1]Department of Functional Genomics, Center for Neurogenomics and Cognitive Research (CNCR), VU University, Amsterdam, The Netherlands and [2]Department of Human Genetics, CNCR, Amsterdam UMC, Amsterdam, the Netherlands
corresponding author: Jan R.T. van Weering, De Boelelaan 1085, 1081 HV, Amsterdam, The Netherlands, jan.van.weering@vu.nl, +31 (0) 20 5986930

Keywords: Endosome sorting, neurotransmission, SNX4, hippocampal neurons

Sortin-Nexin 4 (SNX4) is an evolutionary conserved organizer of membrane recycling. In neurons, SNX4 accumulates in synapses, but how SNX4 affects synapse function remains unknown. We generated a conditional SNX4 knock-out mouse model and report that SNX4 cKO synapses show enhanced neurotransmission during train stimulation, while the first evoked EPSC was normal. SNX4 depletion did not affect vesicle recycling or the levels and localization of SNARE-protein VAMP2/synaptobrevin-2. However, SNX4 depletion affected synapse ultrastructure: an increase in docked synaptic vesicles at the active zone, while the overall vesicle number was normal, and a decreased active zone length. These effects together lead to a substantially increased density of docked vesicles per release site. In conclusion, SNX4 is a negative regulator of synaptic vesicle docking and release. These findings suggest a role for SNX4 in synaptic vesicle recruitment at the active zone.

Endosome sorting plays a critical role in the recycling and degradation of proteins in various eukaryotic cell types, including neurons (Cullen & Steinberg, 2018; Huotari & Helenius, 2011; Sardana & Emr, 2021; Vietri et al., 2020). Synapses, in particular, rely on rapid recycling mechanisms to replenish synaptic vesicles (SVs) and facilitate neurotransmitter release (Kononenko & Haucke, 2015; Rizzoli, 2014; Südhof, 2000). The extent to which endosome sorting is involved in these processes has been a subject of ongoing debate since the early studies on SV recycling (Ceccarelli et al., 1973; Heuser & Reese, 1973; Kononenko & Haucke, 2015; Watanabe & Boucrot, 2017). While it has been demonstrated that depleting endosomal proteins affect neurotransmitter release (Chen et al., 2017; Tagliatti et al., 2016; Uytterhoeven et al., 2011), the precise role of these sorting proteins on SV maintenance and fusogenity remains not well understood.

Sorting nexins (SNXs) are evolutionary conserved organizers of endosome sorting that are recruited to endosome membrane domains by a phox homology (PX) domain (Carlton et al., 2005). SNX4 belongs to a subgroup of SNXs containing a C-terminal a Bin–Amphiphysin–Rvs (BAR) domain that recognizes and remodels curved endosome membranes (Cullen & Steinberg, 2018; Teasdale et al., 2001; Van Weering et al., 2012). While several SNX-BARs are associated with the retromer-related Endosomal SNX-BAR Sorting Complex for Promoting Exit (ESCPE)-1 (Simonetti et al., 2023), SNX4 forms a distinct sorting complex with SNX7, SNX30 (Antón et al., 2020; van Weering et al., 2012), SNX5 (Zhou et al., 2022), or SNX32 (Sugatha et al., 2023) for endosome-to-cell surface recycling pathways and autophagosome traffic (Traer et al., 2007; Van Weering et al., 2012; Zhou et al., 2022). SNX4 emerges as a central hub in this endosome recycling pathway as the expression of SNX4 is required for the stable SNX7 and SNX30 protein levels in cells (Antón et al., 2020). SNX4 is expressed in all cell types but to what extent this conserved principle also operates in highly polarized mammalian cells, such as neurons, remains unclear. In post-mortem AD brain material, altered

protein levels of SNX4 have been observed (Kim et al., 2017). SNX4 is implicated in the recycling of the amyloid precursor protein cleaving enzyme (BACE-1), sorting it away from the endolysosomal pathway (Kim et al., 2017; Toh et al., 2018). Consequently, dysregulation of SNX4 may lead to the mislocalization of BACE-1 to late endosomal compartments, potentially contributing to altered amyloid-ß-production. In yeast, Snx4 is essential for the endosome recycling of Snc1p, a homolog of the SNARE protein VAMP2/synaptobrevin-2 (VAMP2/syb2) that is essential for synaptic transmission (Hettema et al., 2003; Ma et al., 2017; Schoch et al., 2001). In neurons, SNX4 specifically accumulates in synapses, and its knockdown dysregulates protein pathways involved in neurotransmission (Vazquez-Sanchez et al., 2020). While its synaptic subcellular localization has been shown, the functional role of SNX4-dependent endosome sorting in synapses remains unknown.

In this study, we characterize the role of endosomal sorting protein SNX4 in synapse function using a novel conditional SNX4 knock-out mouse model. We show that SNX4 limits synaptic vesicle docking and release. SNX4 depletion enhances neurotransmission specifically during train stimulation, while the first evoked response is not significantly affected. SNX4 depletion does not impact vesicle recycling or the levels and localization of the SNARE-protein VAMP2/syb-2. The overall number synaptic vesicles is unaffected in SNX4 cKO neurons, but these synapses show an increased number of docked synaptic vesicles at the active zone of the presynapse. The active zone length is decreased, thereby further increasing the density of synaptic vesicles at the release site of SNX4 cKO synapses. Our data collectively shows that the endosomal sorting protein SNX4 is a negative regulator of synaptic vesicle docking and release.

RESULTS

Neuronal SNX4 protein levels are depleted in 21 days in conditional SNX4 knock out mouse primary cultures.

We generated a conditional knock-out mouse model for SNX4 (Fig. 1a) to circumvent previously reported off-target effects using shRNA approaches (Vazquez-Sanchez et al., 2020). In neuronal cultures, SNX4 has a half lifetime of 10.6 days (Dörrbaum et al., 2018). To test SNX4 optimal knock out efficiency, cKO neurons were fixed after 21 days *in vitro* (DIV21) and Cre expression was initiated at different time points (DIV7, DIV3, and DIV0) (Fig. 1b). SNX4 expression was detected by western blot which showed a reduction of 67% after 14 days of cre, 83% after 18 days of cre and 90% after 21 days of cre compared to control neurons infected with delta-Cre (Fig. 1c, d). Immunohistochemistry of SNX4 in primary hippocampal neurons showed a 64% reduction in SNX4 in MAP2-neurites after 21 days of expressing cre (Fig. 1e, f). Morphological parameters such as dendrite length, based on MAP2 staining, and synapse number, based on VAMP2 puncta, remained unaffected in SNX4 cKO neurons (Fig. 1 f-h & Fig. 4a). These data show a successful depletion of 90% of endosomal sorting protein SNX4 using a novel conditional knock-out mouse model for SNX4.

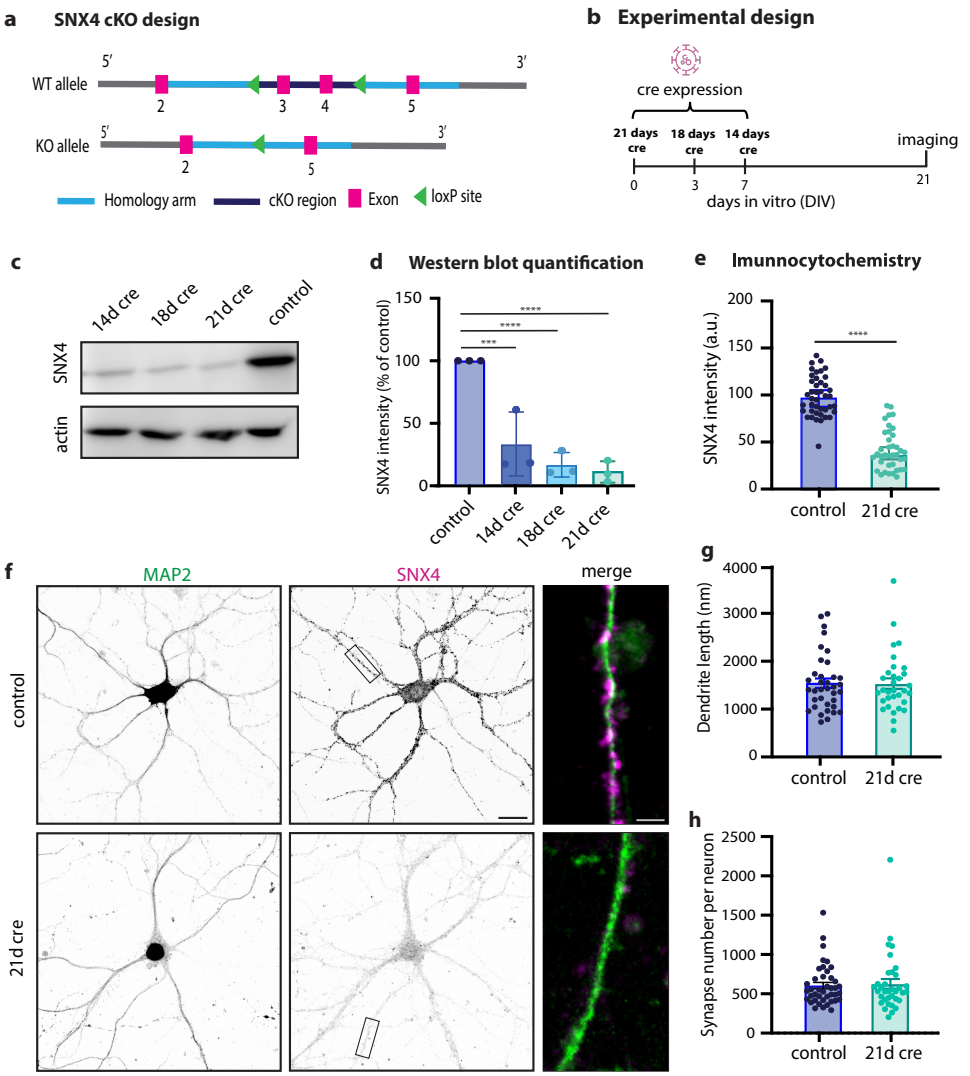

Figure 1: SNX4 is knocked-out in primary hippocampal neurons using a novel conditional knock-out mouse line. (a) Schematic overview of conditional knock-out design of SNX4. **(b)** Schematic overview of experimental design using cre intervention at different DIVs. **(c)** Typical example of western blot of SNX4 and actin at 14 days, 18 days and 21 days of cre and control (delta cre) expression. **(d)** Quantification of western blot SNX4 protein levels for control (dcre), 14 days of cre, 18 days of cre and 21 days of cre, normalized to control. **(e)** Quantification of immunocytochemistry SNX4 intensity normalized to control. **(f)** Typical example of primary hippocampal neurons stained for SNX4 (magenta) and map2 (green) for control and 21 days of cre. Scale bar = 20 µm. Zoom-in scale bar = 3 µm. **(g)** Dendrite length for control and KO hippocampal neurons. **(h)** Number of synapses per neuron (MAP2 mask) based on VAMP2 puncta (shown in Fig. 6) ****p=<0.0001, ***p=0.0003, **p=0.0005, *p=0.0019. Ordinary one-way ANOVA with Tukey's multiple comparisons test for **(d)** with N=3 animals. Mann-Whitney test for **(e)** with n=32-42 neurons per group and N=6 animals and. Data points represent individual western blots/neurons; bar graph represents mean with SEM.

SNX4 depletion enhances neurotransmission during train stimulation

To investigate the functional role of SNX4 in synapses, we studied the effect of SNX4 depletion on neurotransmission by electrophysiological recordings in single hippocampal neurons cultured on glia micro-islands (autapse) at DIV21 (Fig. 2a). Both the amplitude and charge of the first evoked response showed a non-significant trend towards an increase in SNX4 cKO neurons (KO) compared to neurons infected with delta-Cre (control) (Fig. 2b, c & d). The rescue condition where SNX4 was re-expressed at DIV14 (KO + SNX4) showed a decreased amplitude compared to KO but not to control. A similar trend was observed for total charge (Fig. 2b, d). Paired pulse ratios were not affected in SNX4 cKO neurons (Fig. 2e). We next investigated the effect of SNX4 depletion on synaptic transmission during sustained activity using a series of train stimulations at 5, 10 and 40Hz (results in Supplementary table 1, Supplementary Fig S2). During a train of 100 action potentials at 40 Hz, the charge in SNX4 cKO neurons was highly increased (Fig. 2f, h). The average charge between pulse 90-100 was increased by 110% in SNX4 cKO synapses compared to control (Fig. 2g). SNX4 overexpression rescued this increase in charge to WT levels (Fig. 2f, g &h). The size and refilling of the readily releasable vesicle pool (RRP) was estimated using back extrapolation of the cumulative charge (Fig. 2h) (Schneggenburger et al., 1999). While we found no significant

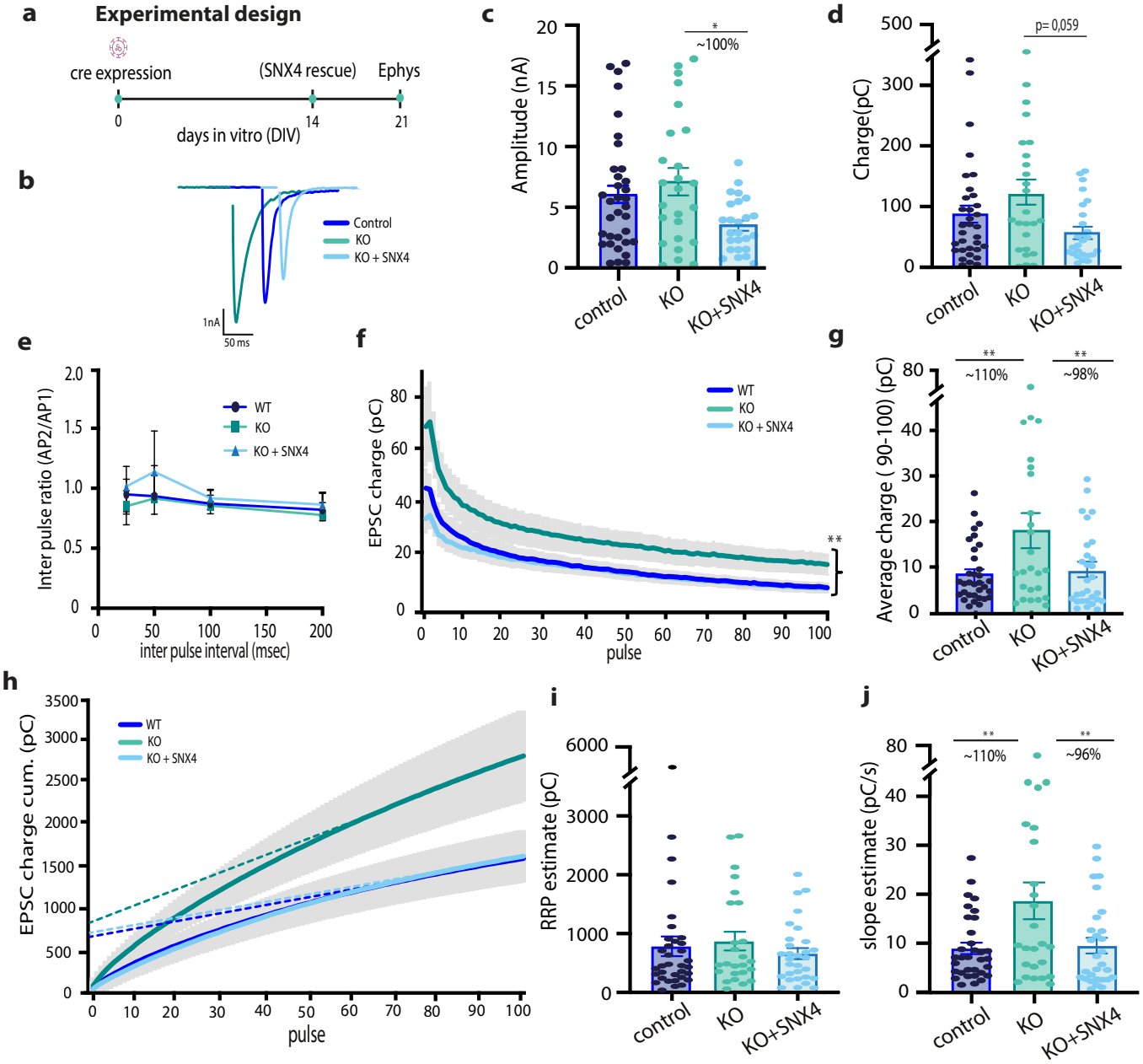

Figure 2: SNX4 depletion increases sustained synaptic vesicle release.
(a) Schematic overview of experimental design using cre intervention at DIV0, SNX4 rescue at DIV14 and recording at DIV21. **(b)** Representative traces of the first evoked response for control, KO and KO+SNX4 upon stimulation. **(c)** Amplitude of first evoked response. **(d)** Charge of first evoked response. **(e)** Paired pulse ratios of amplitude at inter pulse intervals of 25, 50, 100 and 200 msec. **(f)** Mean EPSC charge trace for 100 AP at 40 Hz train. **(g)** Average charge at pulse 90-100. **(h)** Cumulative EPSC charge for 100 AP at 40 Hz train with back extrapolation linear fit to AP 80-100 . **(i)** Estimate of RRP based on back extrapolation (h). **(j)** Estimate of slope based on based on back extrapolation (h). Multilevel ANOVA with n = 25-38 neurons per group of N = 4 animals. ***p < 0.0001, **p < 0.001. Data points represent individual neurons; bar graph represents mean with SEM.

differences in RRP estimate size in SNX4 cKO synapses compared to control (Fig. 2i), the slope estimate of the cumulative charge was increased upon SNX4 depletion, which was rescued by SNX4 overexpression (Fig. 2j). Together these data show enhanced neurotransmission during train stimulation in SNX4 cKO autapses. This suggests that vesicle recruitment during high frequency train stimulation is limited by SNX4.

Synaptic vesicle recycling and retrieval are not altered in SNX4 cKO neurons.

As the recruitment rate of releasable vesicles during train stimulation was increased in SNX4 cKO neurons, we assessed its role in synaptic vesicle recycling using the synaptic vesicle fusion reporter synaptophysin-super-ecliptic-pHluorin (SypHy) (Granseth et al., 2006). Neurons were stimulated by two trains of 100 action potentials at 40 Hz. The total pool of SypHy in acidified SVs per synapse was determined by NH4 superfusion (Fig. 3a, b). SNX4 cKO neurons showed a higher fluorescence intensity upon both stimulation trains (Fig. 3c), represented as the release fraction (Fig. 3d, e), and return to baseline fluorescence level within 60 seconds over a total imaging time course of 160 seconds (Fig. 3c). The fluorescence decay time constant tau in the 60 s after electrical stimulation, a measure for SV endocytosis, was not changed after both stimuli in SNX4 cKO neurons (Fig. 3f). Finally, the responding fluorescent puncta during action potential stimulation as a ratio of the total fluorescent puncta during NH4, the percentage of active synapses, showed a trend towards fewer active synapses in SNX4 cKO neurons (Fig. 3g). Hence, these data show that SNX4 depletion enhances synaptic vesicle release without altering synaptic vesicle recycling and the number of active synapses in hippocampal neurons.

It has, however, been shown that different SV recycling pathways dominate at different temperatures (Watanabe et al., 2013). To test if SNX4 affects SV recycling at physiological temperatures, we used FM4-64 dye loading protocol before electrical field stimulation (Fig. 3h). Recycling SVs were labelled by a 60s-incubation with FM4-64 in 60mM K^+ at 37^0C. Vesicle fusion was triggered by a train of action potentials at 40 Hz, resulting in a decreased FM4-64 fluorescence intensity (Fig. 3h, i). SNX4 cKO neurons showed a similar fluorescence intensity decay after electrical stimulation over a total imaging time course of 80 seconds (Fig. 3j). The average fluorescence signal in the last 10 seconds normalized to baseline (F/F0), a measure for the total amount of recycling synaptic vesicles fusing, was not significantly different between control and SNX4 cKO neurons (Fig. 3k). FM4-64 uptake, a measure for endocytosis at 37 C, was also not altered in SNX4 cKO neurons (Fig. 3l). Taken together, these data suggest that SNX4 depletion does not affect synaptic vesicle endocytosis and recycling both at room temperature and physiological temperature.

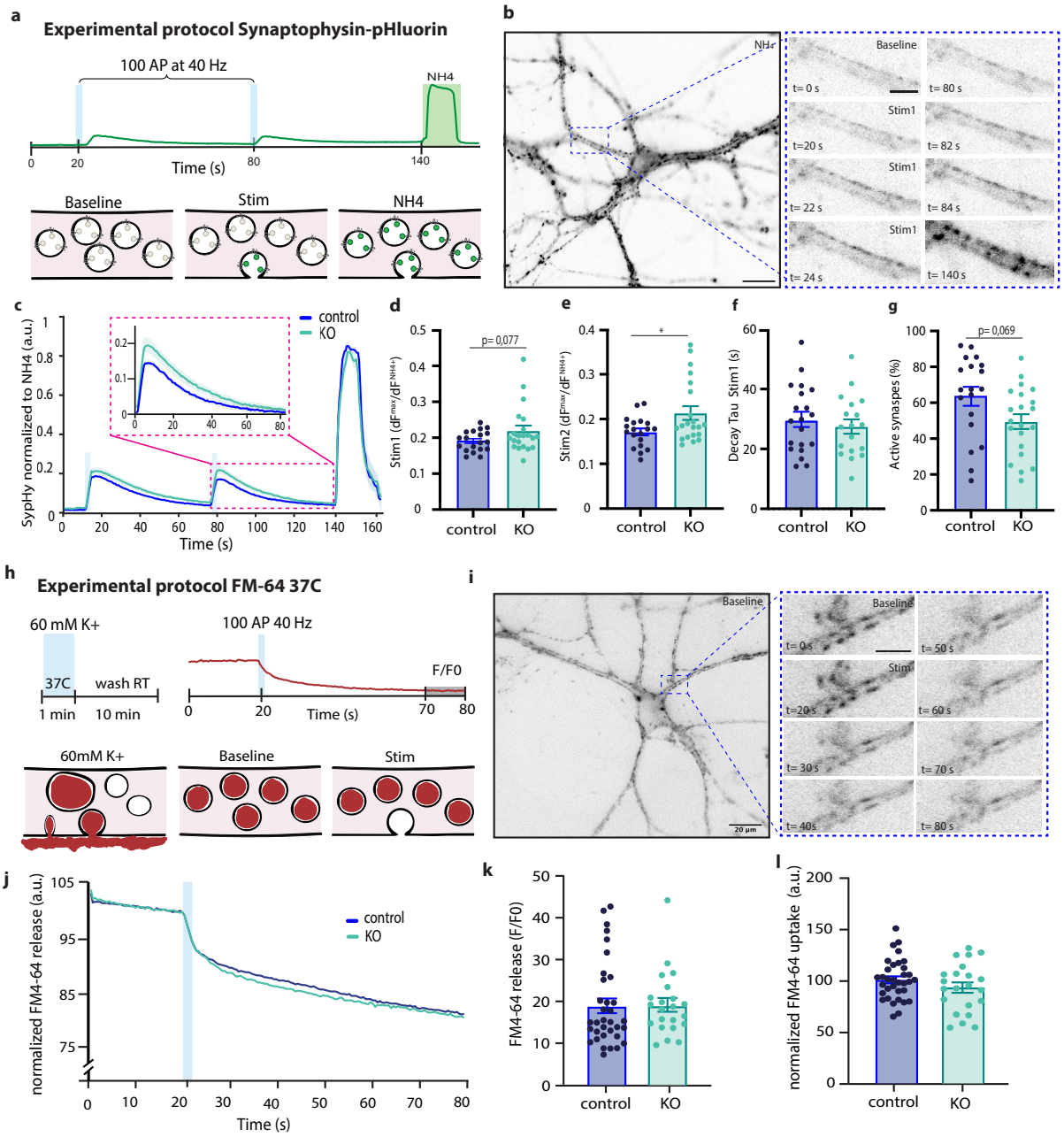

Figure 3: SNX4 depletion does not affect synaptic vesicle recycling at room temperature and physiological temperatures. **(a)** Stimulation paradigm with a single vesicle fluorescence intensity trace**. (b, Left)** Representative image of a Syphy-pHluorin–infected neuron during Tyrode's NH4 application (Scale bar: 20 µm.). **(Right)** Neurite before (baseline) and during (100 AP at 40 Hz) stimulation and during NH4 application (NH4) (Scale bar: 10 µm.). **(c)** The average fluorescence normalized from baseline to maximum Syphy intensity during Tyrode's NH4 application. **(d)** Maximum response amplitude during the first electrical stimulation normalized to maximum NH4 response plotted as $\Delta F^{max}/F^{NH4}$**. (e)** Maximum response amplitude during the second electrical stimulation normalized to maximum NH4 response plotted as $\Delta F^{max}/F^{NH4}$**. (f)** Fluorescence decay time constant tau in the 60 s after electrical stimulation representing SV endocytosis and acidification **(g)** Percentage active synapses. **(h)** Stimulation paradigm with a single vesicle fluorescence intensity trace**.** Recycling SVs are labelled by 60s-incubation with FM4-64 in 60mM K+ at 37C, followed by a 10min washout. Electrical field stimulation (100AP, 40Hz) triggers SV exocytosis recorded as decreased FM4-64 fluorescence intensity. **(i, Left)** Representative image of FM64-dye endocytosed by a neuron during baseline (Scale bar: 20 µm.). **(Right)** Neurite before (baseline) and during (100 AP at 40 Hz) stimulation (Scale bar: 10 µm.). **(j)** The average FM4-64 fluorescence traces, normalized to control baseline, over time showing initial SV loading, followed by release after electrical field stimulation. **(k)** FM4-64 release upon electrical field stimulation **(l)** FM4-64 uptake (upon 60 mm K^+ incubation). Multilevel ANOVA with N=3 animals and n=21-24 neurons per group for Syphy-pHluorin experiment and N=4 animals with n=28-36 neurons per group for FM64-dye experiment. Bar graph represents mean with SEM. Data points represent individual fields of view**.**

SNX4 depletion does not mediate VAMP2/syb-2 levels and distribution.

In yeast it is reported that SNX4 homologue Snx4p mediates retrieval of Snc1p, yeast's VAMP2/syb-2 homologue (Hettema et al., 2003; Ma et al., 2017). Missorting of VAMP2 in neurons could affect synaptic transmission. Therefore, we investigated VAMP2/syb-2 as potential cargo of SNX4. To test whether SNX4 mediates VAMP2/syb-2 retrieval in neurons, we investigated the localization, number and expression levels of VAMP2/syb-2 upon SNX4 knock-out by immunohistochemistry. SNX4 immunostaining showed clear co-localization with VAMP2/syb-2 (Fig. 4a). In SNX4 cKO neurons, no significant difference was found in VAMP2/syb-2 puncta number per µm dendrite or VAMP2/syb-2 intensity (Fig. 4a, b, c). Sholl-analysis of average VAMP2/syb-2 intensity over distance from soma also revealed no differences in VAMP2/syb-2 localization upon SNX4 depletion (Fig. 4d). Western blot analysis revealed no changes in total VAMP2/syb-2 protein levels (Fig. 4e). These data show that SNX4 is not required for a normal VAMP2/syb-2 distribution and protein level, as observed for the yeast orthologs of both proteins.

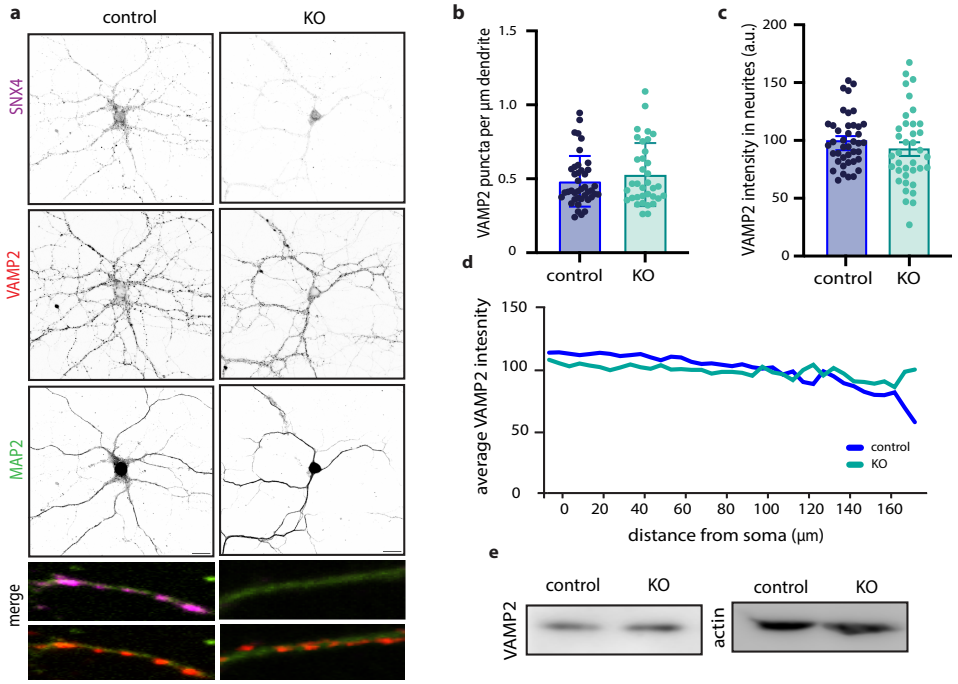

Figure 4: SNX4 depletion does not decrease VAMP2 levels and localization. (a) Typical example immunocytochemistry images of primary hippocampal neurons stained for SNX4 (magenta), VAMP2 (red) and MAP2 (green) from control and SNX4 cKO mice. Scale bar = 20 µm. Merge zoom-in scale bar = 2 µm. **(b)** VAMP2 puncta per µm dendrite for control and KO. **(c)** VAMP2 intensity measured in dendrites. **(d)** Sholl analysis of average VAMP2 intensity over distance from the soma for control and KO. **I** Western blot of SNX4, VAMP2, and actin for control and KO. Data points represent individual neurons, N=6 animals and n=35-41 neurons for VAMP2 data, bar graphs represent mean with SEM.

Presynaptic ultrastructure and synaptic vesicle docking are affected in SNX4 cKO synapses.

Next, we sought to further investigate synapse organization upon SNX4 depletion using electron microscopy (Fig 5a). The number of docked vesicles was measured by direct contact of vesicles with the active zone plasma membrane (Fig. 5a,b). The average synaptic vesicle size, defined by all clear core vesicles smaller than 50 nm, was reduced by 5%, whereas vesicles larger than 50 nm, did not show significant changes upon SNX4 depletion (Fig. 5c, d). In SNX4 cKO synapses, the number of docked vesicles was significantly higher than in control (Fig. 5a, f) whilst the total number of vesicles was not altered (Fig. 5e). When normalized to the active zone length, the density of docked vesicles at the active zone length further increases by 50% in SNX4 cKO synapses compared to control (Fig. 5g). Moreover, we observed a significant decrease in active zone length, PSD length and vesicle cluster area (Fig. 5g-j). Together these data show that SNX4 depletion affects the presynaptic ultrastructure, characterized by smaller active zone length and vesicle cluster area, suggesting a decrease in overall synapse size. In

these smaller synapses, SNX4 cKO neurons contain more docked synaptic vesicles leading to a substantially increased density of docked vesicles per release site.

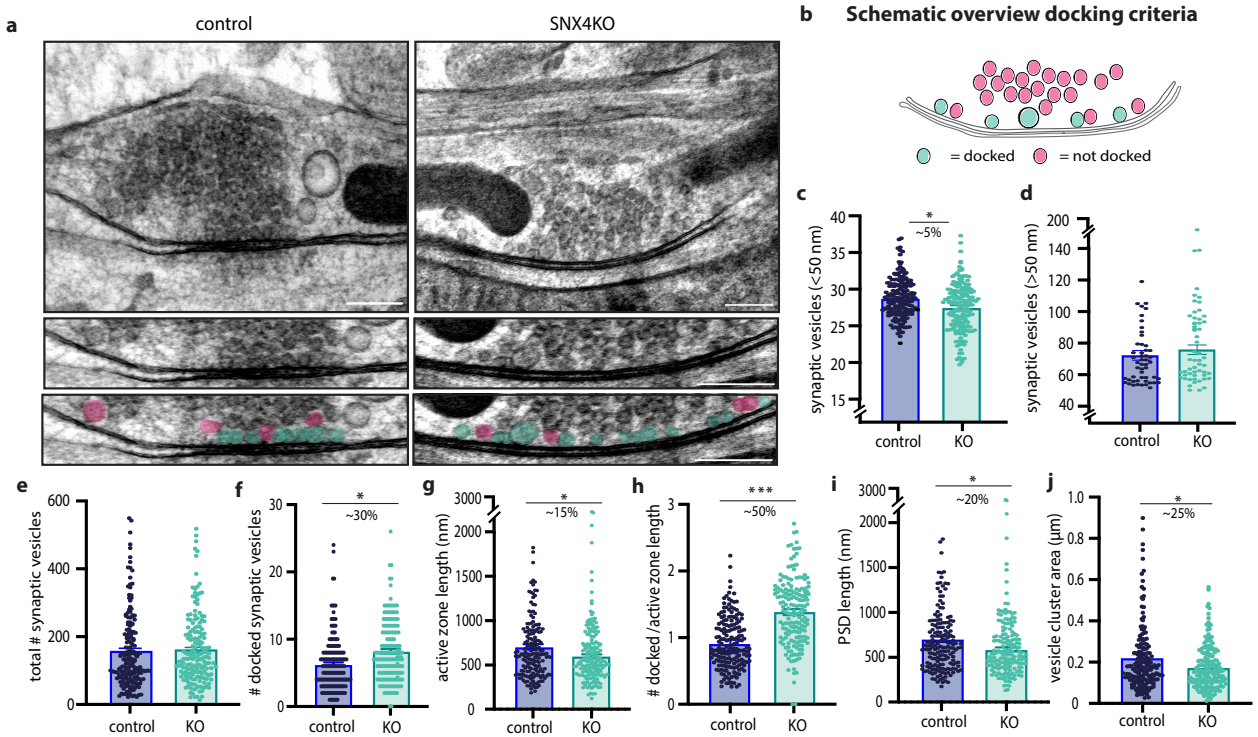

Figure 5: SNX4 depletion increases the number of docked vesicles at the active zone. (a) Example micrographs of control and SNX4 cKO synapses (Scale bar: 200 nm) with zoom in on the active zone region indicating docked (blue) and non-docked vesicles (pink) (Scalebar : 100 nm) **(b)** Schematic overview of docked and undocked vesicles. **(c & d)** The average vesicle size, distinguished between synaptic vesicles (<50 nm) and larger clear core vesicles (>50 nm). **(e)** The total amount of synaptic vesicles in the synaptic cloud. **(f)** The number of docked synaptic vesicles in control and SNX4 cKO synapses**. (g)** The active zone length. **(h)** The number of docked vesicles normalized to active zone length**. (i)** The post synaptic density (PSD) length. **(j)** The area of the vesicle cloud in control and SNX4 cKO synapses. Bar graphs represent mean with SEM with n = 174-175 synapses per group of N = 3 animals. Data points are individual synapses. ***p < 0.0001, **p < 0.001 using Mann-Whitney test.

Discussion

In this study we addressed the role of SNX4-dependent endosome sorting in synapses, using a new conditional SNX4 knock-out mouse model. We show that SNX4 cKO synapses elicit enhanced neurotransmission during train stimulation. SNX4 depletion did not affect vesicle recycling or the levels and localization of SNARE-protein VAMP2/syb-2. Electron microscopy showed that synapses had an increased number of docked vesicles at the active zone, while the overall number of synaptic vesicles was normal. The active zone length was decreased upon SNX4 depletion, thereby further increasing the density of docked synaptic vesicles at the release site. Taken together, our data shows that the endosomal sorting protein SNX4 is a negative regulator of synaptic vesicle docking and release. These findings indicate that SNX4 regulates synaptic vesicle recruitment at the active zone.

Enhanced SV recruitment and increased SV docking explain increased transmission in SNX4 cKO synapses

SNX4 cKO synapses showed a 110% increase in neurotransmission during intense stimulation (Fig. 2f). A trend towards increased neurotransmission was observed already from the start of

237 the train, and also in single evoked responses (Fig. 2c-d), but became more prominent (and
238 significant) during sustained stimulation. Despite the variability within all datasets, both trends
239 and the significant effect during sustained stimulation were fully reversed by acute SNX4
240 expression. The total number of synapses (Fig 1h) and fraction of active synapses (Fig 3g) was
241 not affected in SNX4 cKO neurons, suggesting an intrasynaptic effect. While approximately
242 twice more vesicles were released during sustained stimulation in the absence of SNX4 (Fig.
243 2f), our RRP estimation indicated a normal resting state RRP (Fig. 2i). All measures of release
244 probability were normal (normal paired pulse facilitation, Fig. 2e, and shape of the rundown
245 curve, Fig. 2f), indicating that an increased release probability is an unlikely explanation for
246 the observed increase in neurotransmission during sustained stimulation. Hence, this suggests
247 that a higher recruitment rate of SVs to the releasable pool (Fig. 2h,j) in SNX4 cKO synapses
248 is responsible for the increased neurotransmission. While back extrapolation methods for
249 estimating the RRP have their limitations and mechanisms of SV recruitment remain not fully
250 understood, it is evident that the involvement of newly recruited vesicles becomes more
251 prominent during high frequency trains (Neher et al., 2015). In line with this, the increased
252 neurotransmission of SNX4 cKO neurons was less prominent in 5Hz and 10Hz trains (Fig S2).
253 Hence, an increased contribution of newly recruited vesicles during sustained stimulation is
254 consistent with the fact that neurotransmission is increased especially during high frequency
255 stimulation in SNX4 cKO synapses.
256 The increase in neurotransmission during sustained stimulation was also observed with
257 synaptic vesicle fusion reporter synaptophysin-pHluorin but not with the FM-64 dye. The latter
258 method reports the release of only recycled vesicles, suggesting that these do not contribute to
259 the enhanced release. Finally, examining SV recycling with FM-64 dye indicates that the
260 increased SV recruitment in SNX4 cKO synapses is not driven by an enhanced rate of the
261 synaptic vesicle cycle, as endocytosis and release of recycled SVs were normal in SNX4 cKO
262 synapses.
263
264 Ultrastructural characterization of SNX4 cKO synapses revealed a 50% increase in docked
265 vesicles when normalized to active zone length. This increase might contribute to an enhanced
266 SV recruitment and support increased neurotransmission in SNX4 cKO synapses. If vesicles
267 are already docked, they may be recruited faster during train stimulation. Synaptic vesicle
268 docking appears to be a more dynamic process than previously conceived, where docked SVs
269 are dynamically replaced by recruited vesicles from various synaptic vesicle pools, a process
270 depending on activity (Kusick et al., 2020).An increase in docked SV concentration at the
271 active zone also implies a closer proximity to calcium channels. However, all measures of
272 release probability were unaffected by SNX4 deficiency (as argued above) suggesting a normal
273 channel coupling in SNX4 cKO synapses.
274
275 **SNX4 at the crossroad of endosomal sorting and autophagy regulating synaptic output.**
276
277 Increased neurotransmission upon depletion of endosomal genes has been shown by several
278 labs (Fernandes et al., 2014; Soykan et al., 2021; Tagliatti et al., 2016; Uytterhoeven et al.,
279 2011). These results are consistent with a postulated hypothesis that endosomes act sorting
280 stations for SV proteins and control the balance between novel and reused SV proteins that
281 affect SV release and neurotransmission efficiency (Fernandes et al., 2014; Truckenbrodt et
282 al., 2018; Uytterhoeven et al., 2011).
283 In the presence of SNX4, the recycling process may lead to the re-use of older SV
284 proteins that, as indirect consequence, potentially diminish the efficiency of SV exocytosis. In
285 the absence of SNX4, older SV proteins are less recycled and traffic towards degradation,
286 rendering the synapse with relatively more novel SV proteins, enhancing SV recruitment and

fusion. Blocking the degradation pathway with HOPS/ESCRT mutants rescues the observed increased release (Fernandes et al., 2014; Uytterhoeven et al., 2011) . Similarly, Skywalker and ARF6 mutants show increased SV sorting through endosomal intermediates, increasing SV docking and release (Fernandes et al., 2014; Tagliatti et al., 2016; Uytterhoeven et al., 2011). Our data is consistent with this literature, demonstrating enhanced neurotransmission upon inactivation of an endosome sorting gene. That said, SNX4 cKO synapses do not show an accumulation of endosomal intermediates (Fig 5d) or decreased SV numbers (Fig 5e) as reported for other endosome gene mutants, marking a novel finding in endosomal protein knockout studies.

Endosomal sorting also mediates the delivery of active zone proteins, where disturbances in these pathways potentially correlate with smaller active zones and SVs, ultrastructural phenotypes we also observed in SNX4 cKO synapses. Previous studies suggest that the removal of SNX4 directs its cargo toward the degradative pathway (Hettema et al., 2003; Traer et al., 2007). Although the SNX4 cargo, particularly in mammalian neurons, is currently unknown, it is unlikely that VAMP2/syb-2 recycling explains our phenotype since the overall levels and localization of VAMP2/syb-2 remained unaffected upon SNX4 depletion.

Apart from endosome sorting, SNX4 has been reported to regulate several types of autophagy (Antón et al., 2020; Hanley et al., 2021; Zhou et al., 2022). Recent literature has shown that synaptic vesicle release could be regulated by synaptic autophagy (reviewed by Decet & Verstreken, 2021). Loss of ATG5 has been shown to result in increased neurotransmission, an effect independent from total SVs pool number (Kuijpers et al., 2021). Knock down of SNX4 altered recruitment and turnover kinetics of ATG5 (Antón et al., 2020), which might also impact on neurotransmitter release. Collectively, both endosome sorting and autophagic pathways highlight the importance of SV protein turnover in maintaining efficient neurotransmitter release, with potential regulatory contributions from SNX4.

SNX-BAR proteins critical for synapse function.

Many of our examined synaptic parameters remained unaltered or showed considerable variability, including our hypothesis that depletion of a synaptic endosomal sorting protein would disrupt synaptic recycling. This suggests the presence of redundant pathways compensating for SNX4 depletion, potentially involving other SNX-BAR complexes or endosomal sorting complexes like ESCPE, retriever, or retromer (Simonetti et al., 2023). Particularly SNX-BAR proteins, such as SNX7 and SNX30, are of potential interest for future research due to their ability to form selective complexes with SNX4 (Antón et al., 2020). The role of endosome sorting in the synaptic vesicle cycle is increasingly recognized through knockout studies targeting various endosomal complexes, revealing changes in SV exocytosis, SV endocytosis, or endosome-like vesicle numbers (X. Chen et al., 2017; X. W. Chen et al., 2008; Inoshita et al., 2017; Tagliatti et al., 2016). Our data supports this, showing for the first time that a protein from the highly evolutionary conserved SNX-BAR protein family, such as SNX4, regulates SV docking at the active zone and sustained SV release. Taken together, we show that endosomal sorting protein SNX4 regulates synaptic vesicles recruitment at the active zone. The precise regulation of vesicle availability is crucial for a synapse to effectively coordinate neurotransmission, a process heavily relying on endosome sorting mechanisms.

MATERIAL&METHODS

Laboratory animals and primary neuron cultures

Animals were housed and bred according to institutional and Dutch governmental guidelines (DEC-FGA 11-03 and AVD112002017824). The SNX4 conditional KO targeting strategy resulted in flanking exon 3 and 4 to achieve loss of function of the mouse SNX4 gene (Suppl. Fig 1a). Dissociated hippocampal neuron cultures were prepared from P01 SNX4KO mouse embryos. Hippocampi dissected free of meninges in Hanks' balanced salt solution (Sigma, H9394) supplemented with 10 mM HEPES (Gibco, 15630- 056). The hippocampi were isolated from the tissue and digested with 0.25% trypsin (Gibco, 15090-046) in Hanks' HEPES for 20 min at 37°C. Hippocampi were washed three times with Hanks' HEPES and triturated with fire-polished glass pipettes. Neurons were counted and plated in Neurobasal medium (Gibco, 21103-049) supplemented with 2% B-27 (Gibco, 17504-044), 1.8% HEPES, 0.25% Glutamax (Gibco, 35050-038), and 0.1% penicillin–streptomycin (Gibco, 15140-122). Hippocampal neurons were plated in 12-well plates at a density of 25.000 cells per well on 18-mm glass coverslips containing rat glia or 50.000 cells on coverslips containing 0.01% Poly-ornithin (Sigma P4957) and 2.5 ug/ml laminin coating (Sigma L2020) solution o/n at RT. Neuronal cultures were kept in supplemented Neurobasal at 37°C and 5% CO2 until DIV21.

Constructs and lentiviral infection

Neuronal cultures were infected with EGFP-Cre and EGFP-control (delta Cre) at DIV0 to generate SNX4KO. All constructs were cloned into lentiviral vectors under the synapsin promoter, and lentiviral particles were generated following the protocol previously described in (Naldini et al., 1996).The presence of an EGFP nuclear localization sequence (NLS) allowed identification of tranduced cells (Kaeser et al., 2011). For synaptic vesicle release experiments, neurons were infected with Synaptophysin-pHluorin lentivirus at DIV7. Titration of lentiviral particle batches was performed by assessment of number of fluorescent cells upon infection to ensure 100% infection efficiency.

Western blot

Cortical neurons at DIV21 were washed with phosphate-buffered saline (PBS) and lysed in Laemmli sample buffer consisting of 2% SDS (VWR chemicals, M107), 10% glycerol (Merck, 818709), 0.26 M b-mercaptoethanol (Sigma, M3148), 60 mM Tris-HCl (Serva, 37180) pH 6.8, and 0.01% Bromophenol blue (Applichem, A3640). Samples of 450.000 neurons run in SDS-PAGE (10% 1 mm acrylamide gel with 2, 2, 2-Trichloroethanol) using standard SDS-PAGE technique and transferred into polyvinylideenfluoride membranes (Bio-rad) (1 hour, 0.25 mA, 4 C°). Blots were blocked and incubated with primary antibodies (4 degrees O/N) in PBS containing 0.1% Tween-20 (Sigma, P2287) (PBS-T) and 5% milk. Primary antibodies included polyclonal rabbit SNX4 (1:500; SySy, Cat. No. 392 003), monoclonal mouse actin (1:10000; Chemicon, Cat. No. MAB1501), monoclonal mouse VAMP2/synaptobrevin2 (1:2000; SySy, CL 69.1), and polyclonal rabbit BACE-1 (1:500; Abcam ab20770). After washing with PBS-T, blots were incubated with secondary horseradish peroxidase (HRP)-labeled antibodies (1:10000; Sigma) in PBS-T and 5% milk (1 hour, RT). After washing with PBS-T, blots were developed with SuperSignal West Femto substrate (Thermo Scientific, 11859290) for 2 min. Chemiluminescence labelled proteins were visualised with the Odyssey Imaging System (LI-COR) for appropriate times and analysed with Image Studio 5.2 software (LI-COR) or ImageJ.

387 **Immunocytochemistry**
388
389 Neurons at DIV21 were fixed in 3.7% formaldehyde (Electron Microscopies Sciences, 15680)
390 in PBS, pH 7.4, for 25 min at RT. After washing with PBS, cells were permeabilized for 5 min
391 with 0.5% Triton X- 100 (Fisher Chemical, T/3751/08)–PBS and incubated for 30 min with
392 PBS containing 2% normal goat serum (Gibco, 16210-072) and 0.1% Triton X-100 to block
393 nonspecific binding. Incubations with primary antibodies were performed O/N at 4°C. After
394 PBS washing steps incubations with secondary antibodies followed for 1h at RT. Primary
395 antibodies included polyclonal rabbit SNX4 (1:500; SySy, Cat. No. 392 003), monoclonal
396 mouse VAMP2/synaptobrevin2 (1:1000; SySy, CL 69.1), and polyclonal chicken MAP2
397 (1:300; Abcam ab5392) and Alexa Fluor conjugated secondary antibodies (1:1000;
398 Invitrogen). Coverslips were mounted with Dabco-Mowiol 4-88 (Sigma, 81381) and confocal
399 microscope (Nikon eclipse Ti) using a 40× oil immersion objective (NA = 1.3)) was used to
400 examine the samples. Laser settings were kept constant within experimental conditions.

401 **Electrophysiological recordings**

402 Autaptic cultures of *SNX4* null neurons were grown for 21–25 days before measuring. Whole-
403 cell voltage-clamp recordings (V_m = −70 mV) were performed at room temperature with
404 borosilicate glass pipettes (2.5–4.5 mOhm) filled with 136 mM KCl, 17.8 mM HEPES, 0.6
405 mM $MgCl_2$, 4 mM ATP-Mg, 0.3 mM GTP-Na, 12 mM phosphocreatine dipotassium salt, 45.3
406 mM phosphocreatine kinase, and 1 mM EGTA (pH 7.30). External solution contained the
407 following (in mM): 10 HEPES, 10 glucose, 140 NaCl, 2.4 KCl, 4 $MgCl_2$, and 4 $CaCl_2$ (pH =
408 7.30, 300 mOsmol). Recording was acquired with an MultiClamp 700B amplifier (Molecular
409 Devices), Digidata 1550B, and Clampex 9.0 software (Molecular Devices). After whole-cell
410 mode was established, only cells with an access resistance of < 15 MΩ and leak current of <
411 300 pA were accepted for analysis. Serie resistance compensation was between 70-80%.
412 Access resistance was measured before and after recordings. Recordings with a > 20% increase
413 in access resistance were excluded from analysis, as well as recordings that showed voltage
414 clamp escape or clipping. GABAergic recordings were identified based on their postsynaptic decay
415 kinetics and excluded. EPSCs were elicited by a 1-ms depolarization to 30 mV. RRP and slope
416 estimates were obtained by a linear fit of cumulative total charge plot from pulse 80 to 100 for
417 each individual cell with y-intercept for RRP estimate and slope as recruitment rate estimate
418 (Schneggenburger et al., 1999).

419 **Live cell imaging**
420
421 Live imaging experiments were performed at DIV21 on a custom build imaging microscope
422 (IX81; Olympus) with an MT20 light source (Olympus) with a 40× oil objective (NA=1.3)
423 appropriate filter sets (semrock, Rochester, NY) and an EM charge-coupled device camera
424 (C9100-02; Hamamatsu Photonics, Japan). Xcellence RT imaging software (Olympus)
425 controlled the microscope and image acquisition. Coverslips were perfused with Tyrode's
426 solution (119 mM NaCl, 2.5 mM KCl, 2 mM $CaCl_2^{-}$ 2H2O, 2mM $MgCl_2^{-}$ 6H2O, 25 mM
427 HEPES, and 30 mM glucoseH2O, pH 7.4, mOsmol 280). For synaptic vesicle release
428 experiments, time-lapse (2 Hz) recordings consisted of 30 s baseline recordings followed by
429 two electrical field stimulations with 60s recovery time in between and a final stimulation 10s
430 of NH4-Tyrode's perfusion (2 mM $CaCl_2$, 2.5 mM KCl, 119 mM NaCl, 2 mM $MgCl_2$, 30 mM
431 glucose, 25 mM HEPES, 50 mN NH4Cl at pH 7.4). Electrical field stimulation was applied via
432 parallel platinum electrodes powered by a stimulus isolator (WPI A385) delivering 30-mA, 1-
433 ms pulses, regulated by a Master-8 pulse generator (A.M.P.I.) providing 100 APs at 40 Hz with

434 a 0.5-s interval. Glass capillaries close to the isolated neuron were used for chemical
435 stimulation. For the FM4-64 experiments, neurons were pre imaging incubated in high
436 potassium Tyrode's for 10 min at 37 C°(61.5 mM NaCl, 60 mM KCl, 2 mM CaCl22H2O,
437 2mM MgCl2 6H2O, 25 mM HEPES and 30 mM glucoseH2O, pH 7.4, mOsmol 280).
438
439 **Imaging analysis**
440
441 Timelapse recordings stacks were used to analyze SyPhy and FM4-64 fusion events (2 Hz,
442 1000 × 1000pixels). In ImageJ fusion events were selected manually and fluorescence traces
443 were measured in a circular 3 × 3 pixel ROI (0.6 x 0.6 um), somatic events not included. ROI
444 intensity measures of SyPhy puncta were exported to a custom-built Matlab program for
445 semiautomated detection of fusion events and duration. Fluorescence traces from the ROI were
446 expressed as fluorescence change (deltaF) compared to initial fluorescence (F0), with the
447 average of frames 1-10 for determining F0. Fusion events were automatically detected when
448 displaying a sudden increase of two standard deviations above F0. Synaptic vesicle pool
449 numbers and synapses were estimated using MAP2 mask in automated image analysis software
450 SynD. Active synapses were determined by 3x SD over baseline. Synapse detection settings
451 were optimized to measure SyPhy and VAMP2/syb-2 puncta signal and kept constant within
452 the same dataset. For FM4-64 puncta, fluorescence traces were expressed as change (DF)
453 compared to baseline fluorescence (F0) and the average of the last 10 frames was used to
454 determine the maximum FM4-64 release.

455 **Cryofixation electron microscopy**

456 Dissociated hippocampal neurons (5000 k/well) from SNX4 cKO mice were plated on pre-
457 grown cultures of rat glia on sapphire disks (Wohlwend GmbH) to form micro-networks of 2–
458 10 neurons per sapphire disk. Prior to cell culture, sapphire disks were etched for 30 minutes
459 in 60% sulfuric acid, washed, incubated in 3M KOH overnight, washed and dried before carbon
460 coating and subsequent baking at 180 C for 2 hours. Sapphire discs were coated by a mixture
461 of 0.1 mg/ml poly-d-lysine (Sigma), 0.7 mg/ml rat tail collagen (BD Biosciences), and 10 mM
462 acetic acid (Sigma) and placed in an agarose-coated 12-well plate to form glia monolayer
463 islands selectively on sapphire disks. The sapphire disks were cryofixed in an EM-PACT2
464 (Leica Microsystems) high-pressure freezer in 5% trehalose/10% BSA in 0.05M phosphate
465 buffer pH 7.4 320 mOsm cryoprotectant. Frozen samples were postfixed in 1% OsO4/ 5%
466 saturated K4Fe(CN)6 in H2O in acetone at −90°C for 74 hours and brought to 0°C at 5°/h.
467 After a couple washes with ice-cold acetone, the sapphire disks were washed with propylene
468 oxide and with an increasing Epon concentration series. The samples were embedded in fresh
469 Epon overnight and left to polymerize at 65°C for 48 h. Sapphire disks were separated from
470 the Epon by dipping the samples in boiling water and liquid nitrogen and regions with micro-
471 networks were selected by light microscopy. These regions were cut out and mounted on pre-
472 polymerized Epon blocks for ultrathin sectioning. Ultrathin sections (80 nm) were cut parallel
473 to the sapphire disk, collected on single-slot, formvar-coated copper grids, and stained in uranyl
474 acetate and lead citrate. Hippocampal synapses were randomly selected at low magnification
475 using an electron microscope (JEOL1010), and the conditions were blinded. For each
476 condition, the number of docked SVs, total SV number, and active zone length were measured
477 on digital images taken at 80,000-fold magnification using custom-written semiautomatic
478 image analysis software running in Matlab (Mathworks). For all morphological analyses the
479 following requirements were set: clearly recognizable synapses with intact synaptic plasma
480 membranes with a recognizable pre- and postsynaptic area and defined SV membranes. SVs

481 were defined as docked if there was no distance visible between the SV membrane and the
482 active zone membrane.

483 **Statistics**

484 Data are shown as mean +- SEM. Data that violated both normality (Shapiro-Wilk) and
485 homogeneity (Levene test) was tested with the two-sided Mann–Whitney U test. Data
486 exhibiting a normal distribution yet significantly altered variation were tested with Welch's t-
487 test. When assumptions of homogeneity and normality were met, data were tested with
488 Student's t test or one-way ANOVA with Tukey's multiple comparisons test. For the analysis
489 of electron microscopy data, electrophysiology data and live cell imaging (pHluorin and FM
490 dye), the intraclass correlation coefficient (ICC) was calculated for different variables
491 applicable to each experiment such as culture batch, sapphire or synapse originating from the
492 same neuron. If ICC was close to 0.1, indicating that a considerable portion of the total variance
493 can be attributed to e.g. culture week, multilevel analysis was performed to accommodate
494 nested data (Aarts et al., 2014). Bar graphs were plotted as the mean with SEM, where
495 individual data points represent fields of view, neurons or synapses (EM data set).

496 **Acknowlegdements**

497 The authors thank dr. Sander Groffen for help with the conditional knock-out mouse design,
498 Joke Wortel for housing and breeding the mice, Desiree Schut for helping with neuronal
499 cultures, Robbert Zalm for cloning and lentiviral production, Marien P Dekker for assistance
500 with EM analysis. We would like to thank Elise van Bree and Sonia Vazquez-Sanchez for their
501 pioneering work on synaptic release in SNX4 shRNA models. The van Weering lab is
502 supported by Alzheimer Nederland (WE.03-2019-06).

503 **Author contributions**

504 J.P. performed experiments and analyzed the data. N.J.B. and L.N.C collected and analyzed
505 Ephys data. J.R.T.vW collected and analyzed EM data. J.P., M.V. and J.R.T.vW designed the
506 experiments and wrote the manuscript with input of all authors.

507 **References**

508 Aarts, E., Verhage, M., Veenvliet, J. V., Dolan, C. V., & Van Der Sluis, S. (2014). A solution
509 to dependency: using multilevel analysis to accommodate nested data. *Nature*
510 *Neuroscience*, *17*(4), 491–496. https://doi.org/10.1038/NN.3648
511 Antón, Z., Betin, V. M. S., Simonetti, B., Traer, C. J., Attar, N., Cullen, P. J., & Lane, J. D.
512 (2020). A heterodimeric SNX4–SNX7 SNX-BAR autophagy complex coordinates
513 ATG9A trafficking for efficient autophagosome assembly. *Journal of Cell Science*,
514 *133*(14). https://doi.org/10.1242/jcs.246306
515 Carlton, J., Bujny, M., Rutherford, A., & Cullen, P. (2005). Sorting nexins--unifying trends
516 and new perspectives. *Traffic (Copenhagen, Denmark)*, *6*(2), 75–82.
517 https://doi.org/10.1111/J.1600-0854.2005.00260.X
518 Ceccarelli, B., Hurlbut, W. P., & Mauro, A. (1973). Turnover of Transmitter and Synaptic
519 Vesicles at the Frog Neuromuscular Junction. *Journal of Cell Biology*, *57*(2), 499–524.
520 https://doi.org/10.1083/JCB.57.2.499

521 Chen, X., Ma, W., Zhang, S., Paluch, J., Guo, W., & Dickman, D. K. (2017). The BLOC-1
522 Subunit Pallidin Facilitates Activity-Dependent Synaptic Vesicle Recycling. *Eneuro*,
523 *4*(1), ENEURO.0335-16.2017. https://doi.org/10.1523/ENEURO.0335-16.2017
524 Chen, X. W., Feng, Y. Q., Hao, C. J., Guo, X. L., He, X., Zhou, Z. Y., Guo, N., Huang, H. P.,
525 Xiong, W., Zheng, H., Zuo, P. L., Zhang, C. X., Li, W., & Zhou, Z. (2008). DTNBP1, a
526 schizophrenia susceptibility gene, affects kinetics of transmitter release. *Journal of Cell*
527 *Biology*, *181*(5), 791–801. https://doi.org/10.1083/jcb.200711021
528 Cullen, P. J., & Steinberg, F. (2018). To degrade or not to degrade: mechanisms and
529 significance of endocytic recycling. *Nature Reviews Molecular Cell Biology*, *19*(11),
530 679–696. https://doi.org/10.1038/s41580-018-0053-7
531 Decet, M., & Verstreken, P. (2021). Presynaptic Autophagy and the Connection With
532 Neurotransmission. *Frontiers in Cell and Developmental Biology*, *9*.
533 https://doi.org/10.3389/FCELL.2021.790721
534 Fernandes, A. C., Uytterhoeven, V., Kuenen, S., Wang, Y.-C., Slabbaert, J. R., Swerts, J.,
535 Kasprowicz, J., Aerts, S., & Verstreken, P. (2014). Reduced synaptic vesicle protein
536 degradation at lysosomes curbs TBC1D24/sky-induced neurodegeneration. *The Journal*
537 *of Cell Biology*, *207*(4), 453–462. https://doi.org/10.1083/jcb.201406026
538 Granseth, B., Odermatt, B., Royle, S. J. J., & Lagnado, L. (2006). Clathrin-mediated
539 endocytosis is the dominant mechanism of vesicle retrieval at hippocampal synapses.
540 *Neuron*, *51*(6), 773–786. https://doi.org/10.1016/J.NEURON.2006.08.029
541 Hanley, S. E., Willis, S. D., & Cooper, K. F. (2021). Snx4-assisted vacuolar targeting of
542 transcription factors defines a new autophagy pathway for controlling ATG expression.
543 *Autophagy*, *17*(11), 3547. https://doi.org/10.1080/15548627.2021.1877934
544 Hettema, E. H., Lewis, M. J., Black, M. W., & Pelham, H. R. B. (2003). Retromer and the
545 sorting nexins Snx4/41/42 mediate distinct retrieval pathways from yeast endosomes.
546 *EMBO Journal*, *22*(3), 548–557. https://doi.org/10.1093/emboj/cdg062
547 Heuser, E., & Reese, T. S. (1973). Evidence for Recycling of Synaptic Vesicle Membrane
548 during Transmitter Release at the Frog Neuromuscular Junction. *The Journal of Cell*
549 *Biology*, *57*, 15–344.
550 Huotari, J., & Helenius, A. (2011). Endosome maturation. *The EMBO Journal*, *30*(17), 3481–
551 3500. https://doi.org/10.1038/EMBOJ.2011.286
552 Inoshita, T., Arano, T., Hosaka, Y., Meng, H., Umezaki, Y., Kosugi, S., Morimoto, T., Koike,
553 M., Chang, H.-Y., Imai, Y., & Hattori, N. (2017). Vps35 in cooperation with LRRK2
554 regulates synaptic vesicle endocytosis through the endosomal pathway in Drosophila.
555 *Human Molecular Genetics*, *26*(15), 2933–2948. https://doi.org/10.1093/hmg/ddx179
556 Kaeser, P. S., Deng, L., Wang, Y., Dulubova, I., Liu, X., Rizo, J., & Südhof, T. C. (2011).
557 RIM proteins tether Ca2+ channels to presynaptic active zones via a direct PDZ-domain
558 interaction. *Cell*, *144*(2), 282–295. https://doi.org/10.1016/j.cell.2010.12.029
559 Kim, N. Y., Cho, M. H., Won, S. H., Kang, H. J., Yoon, S. Y., & Kim, D. H. (2017). Sorting
560 nexin-4 regulates β-amyloid production by modulating β-site-activating cleavage
561 enzyme-1. *Alzheimer's Research and Therapy*, *9*(1), 4. https://doi.org/10.1186/s13195-
562 016-0232-8
563 Kononenko, N. L., & Haucke, V. (2015). Molecular mechanisms of presynaptic membrane
564 retrieval and synaptic vesicle reformation. In *Neuron* (Vol. 85, Issue 3, pp. 484–496).
565 Cell Press. https://doi.org/10.1016/j.neuron.2014.12.016
566 Kuijpers, M., Kochlamazashvili, G., Stumpf, A., Puchkov, D., Swaminathan, A., Lucht, M.
567 T., Krause, E., Maritzen, T., Schmitz, D., & Haucke, V. (2021). Neuronal Autophagy
568 Regulates Presynaptic Neurotransmission by Controlling the Axonal Endoplasmic
569 Reticulum. *Neuron*, *109*(2), 299-313.e9.
570 https://doi.org/10.1016/J.NEURON.2020.10.005

571 Kusick, G. F., Chin, M., Raychaudhuri, S., Lippmann, K., Adula, K. P., Hujber, E. J., Vu, T.,
572 Davis, M. W., Jorgensen, E. M., & Watanabe, S. (2020). Synaptic vesicles transiently
573 dock to refill release sites. *Nature Neuroscience 2020 23:11*, *23*(11), 1329–1338.
574 https://doi.org/10.1038/s41593-020-00716-1
575 Ma, M., Burd, C. G., & Chi, R. J. (2017). Distinct complexes of yeast Snx4 family SNX-
576 BARs mediate retrograde trafficking of Snc1 and Atg27. *Traffic (Copenhagen,*
577 *Denmark)*, *18*(2), 134. https://doi.org/10.1111/TRA.12462
578 Naldini, L., Blömer, U., Gallay, P., Ory, D., Mulligan, R., Gage, F. H., Verma, I. M., &
579 Trono, D. (1996). In Vivo Gene Delivery and Stable Transduction of Nondividing Cells
580 by a Lentiviral Vector. *Science*, *272*(5259), 263–267.
581 https://doi.org/10.1126/SCIENCE.272.5259.263
582 Rizzoli, S. O. (2014). Synaptic vesicle recycling: steps and principles. *The EMBO Journal*,
583 *33*(8), 788. https://doi.org/10.1002/EMBJ.201386357
584 Sardana, R., & Emr, S. D. (2021). Membrane Protein Quality Control Mechanisms in the
585 Endo-Lysosome System. *Trends in Cell Biology*, *31*(4), 269–283.
586 https://doi.org/10.1016/J.TCB.2020.11.011
587 Schneggenburger, R., Meyer, A. C., & Neher, E. (1999). Released fraction and total size of a
588 pool of immediately available transmitter quanta at a calyx synapse. *Neuron*, *23*(2),
589 399–409. https://doi.org/10.1016/S0896-6273(00)80789-8
590 Schoch, S., Deák, F., Königstorfer, A., Mozhayeva, M., Sara, Y., Südhof, T. C., & Kavalali,
591 E. T. (2001). SNARE function analyzed in synaptobrevin/VAMP knockout mice.
592 *Science*, *294*(5544), 1117–1122.
593 https://doi.org/10.1126/SCIENCE.1064335/SUPPL_FILE/1064335S2_THUMB.GIF
594 Simonetti, B., Daly, J. L., & Cullen, P. J. (2023). Out of the ESCPE room: Emerging roles of
595 endosomal SNX-BARs in receptor transport and host–pathogen interaction. *Traffic*,
596 *24*(6), 234–250. https://doi.org/10.1111/TRA.12885
597 Soykan, T., Haucke, V., & Kuijpers, M. (2021). Mechanism of synaptic protein turnover and
598 its regulation by neuronal activity. *Current Opinion in Neurobiology*, *69*, 76–83.
599 https://doi.org/10.1016/J.CONB.2021.02.006
600 Südhof, T. C. (2000). The synaptic vesicle cycle revisited. *Neuron*, *28*(2), 317–320.
601 https://doi.org/10.1016/S0896-6273(00)00109-4
602 Sugatha, J., Priya, A., Raj, P., Jaimon, E., Swaminathan, U., Jose, A., Pucadyil, T. J., &
603 Datta, S. (2023). Insights into cargo sorting by SNX32 and its role in neurite outgrowth.
604 *ELife*, *12*. https://doi.org/10.7554/eLife.84396
605 Tagliatti, E., Fadda, M., Falace, A., Benfenati, F., & Fassio, A. (2016). Arf6 regulates the
606 cycling and the readily releasable pool of synaptic vesicles at hippocampal synapse.
607 *ELife*, *5*(JANUARY2016), 1–18. https://doi.org/10.7554/eLife.10116
608 Teasdale, R. D., Loci, D., Houghton, F., Karlsson, L., & Gleeson, P. A. (2001). A large
609 family of endosome-localized proteins related to sorting nexin 1. *The Biochemical*
610 *Journal*, *358*(Pt 1), 7–16. https://doi.org/10.1042/0264-6021:3580007
611 Toh, W. H., Cheryl Chia, P. Z., Iqbal Hossain, M., & Gleeson, P. A. (2018). GGA1 regulates
612 signal-dependent sorting of BACE1 to recycling endosomes, which moderates Aβ
613 production. *Molecular Biology of the Cell*, *29*(2), 191.
614 https://doi.org/10.1091/MBC.E17-05-0270
615 Traer, C. J., Rutherford, A. C., Palmer, K. J., Wassmer, T., Oakley, J., Attar, N., Carlton, J.
616 G., Kremerskothen, J., Stephens, D. J., & Cullen, P. J. (2007). SNX4 coordinates
617 endosomal sorting of TfnR with dynein-mediated transport into the endocytic recycling
618 compartment. *Nature Cell Biology*, *9*(12), 1370–1380. https://doi.org/10.1038/ncb1656
619 Truckenbrodt, S., Viplav, A., Jähne, S., Vogts, A., Denker, A., Wildhagen, H., Fornasiero, E.
620 F., & Rizzoli, S. O. (2018). Newly produced synaptic vesicle proteins are preferentially

621 used in synaptic transmission. *The EMBO Journal*, *37*(15), 1–24.
622 https://doi.org/10.15252/embj.201798044
623 Uytterhoeven, V., Kuenen, S., Kasprowicz, J., Miskiewicz, K., & Verstreken, P. (2011). Loss
624 of Skywalker reveals synaptic endosomes as sorting stations for synaptic vesicle
625 proteins. *Cell*, *145*(1), 117–132. https://doi.org/10.1016/j.cell.2011.02.039
626 Van Weering, J. R. T., Sessions, R. B., Traer, C. J., Kloer, D. P., Bhatia, V. K., Stamou, D.,
627 Carlsson, S. R., Hurley, J. H., & Cullen, P. J. (2012). Molecular basis for SNX-BAR-
628 mediated assembly of distinct endosomal sorting tubules. *EMBO Journal*, *31*(23), 4466–
629 4480. https://doi.org/10.1038/emboj.2012.283
630 van Weering, J. R. T., Verkade, P., & Cullen, P. J. (2012). SNX–BAR-Mediated Endosome
631 Tubulation is Co-ordinated with Endosome Maturation. *Traffic*, *13*(1), 94–107.
632 https://doi.org/10.1111/J.1600-0854.2011.01297.X
633 Vazquez-Sanchez, S., Gonzalez-Lozano, M. A., Walfenzao, A., Li, K. W., & van Weering, J.
634 R. T. (2020). The endosomal protein sorting nexin 4 is a synaptic protein. *Scientific*
635 *Reports*, *10*(1). https://doi.org/10.1038/s41598-020-74694-6
636 Vietri, M., Radulovic, M., & Stenmark, H. (2020). The many functions of ESCRTs. *Nature*
637 *Reviews. Molecular Cell Biology*, *21*(1), 25–42. https://doi.org/10.1038/S41580-019-
638 0177-4
639 Watanabe, S., & Boucrot, E. (2017). Fast and ultrafast endocytosis. *Current Opinion in Cell*
640 *Biology*, *47*, 64–71. https://doi.org/10.1016/J.CEB.2017.02.013
641 Watanabe, S., Rost, B. R., Camacho-Pérez, M., Davis, M. W., Söhl-Kielczynski, B.,
642 Rosenmund, C., & Jorgensen, E. M. (2013). Ultrafast endocytosis at mouse hippocampal
643 synapses. *Nature*, *504*(7479), 242–247. https://doi.org/10.1038/nature12809
644 Zhou, C., Wu, Z., Du, W., Que, H., Wang, Y., Ouyang, Q., Jian, F., Yuan, W., Zhao, Y.,
645 Tian, R., Li, Y., Chen, Y., Gao, S., Wong, C. C. L., & Rong, Y. (2022). Recycling of
646 autophagosomal components from autolysosomes by the recycler complex. *Nature Cell*
647 *Biology 2022 24:4*, *24*(4), 497–512. https://doi.org/10.1038/s41556-022-00861-8

648

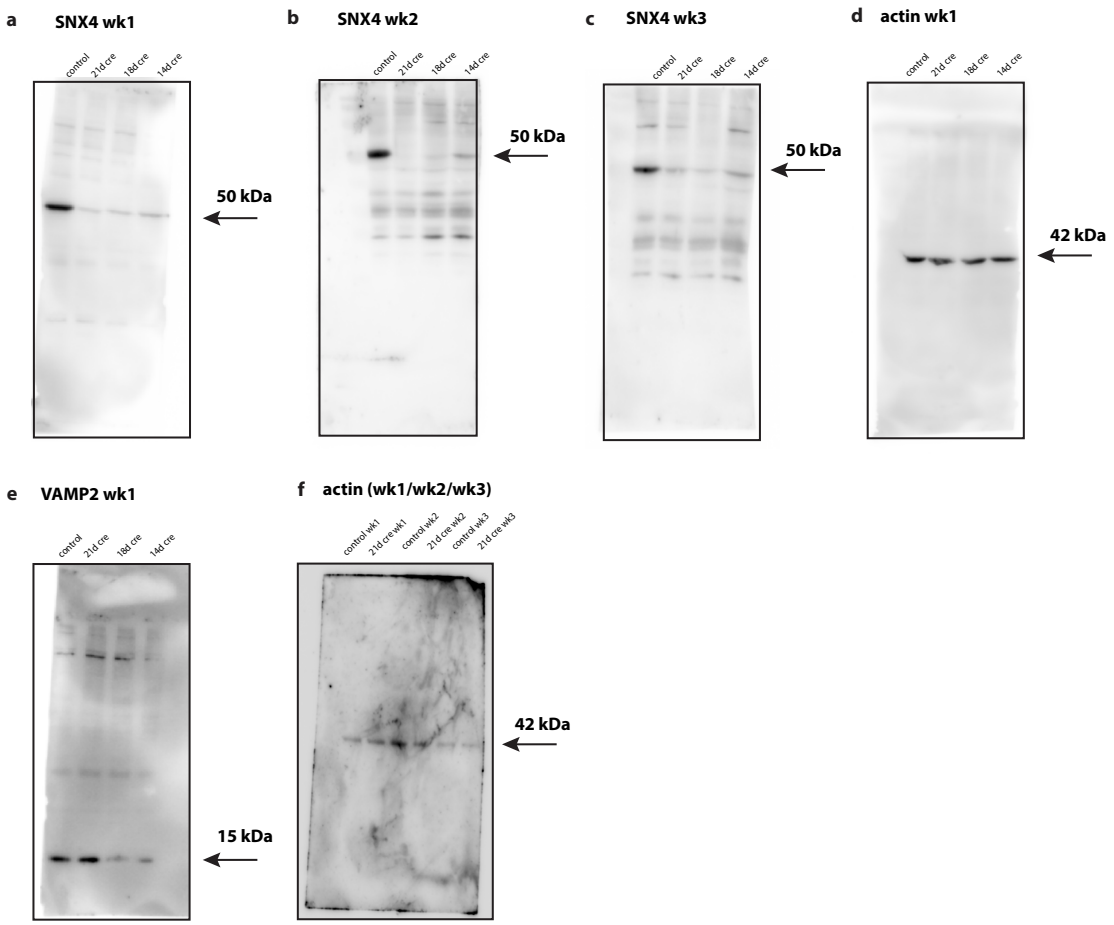

Supplementary figure 1: Overview of uncropped blots used for western blot analysis. (a,b,c) SNX4 at 50Kda for control (21 days of dcre), 21 days of cre, 18 days of cre and 14 days of cre. Repeated for three different animals, wk1 is normalized to actin and wk2 and wk3 are normalized to unspecific band on the blot. Fold of change is determined for all weeks by normalizing to control per week. **(d)** Actin at 42 kD for control, 21 days of cre, 18 days of cre and 14 days of cre. Same animal and transfer as SNX4 wk1. **(e)** VAMP2 at 15 kD for control, 21 days of cre, 18 days of cre and 14 days of cre. Same animal and transfer as SNX4 wk1. **(f)** Actin at 42 kD for control and 21 days of cre for three different animals on one blot.

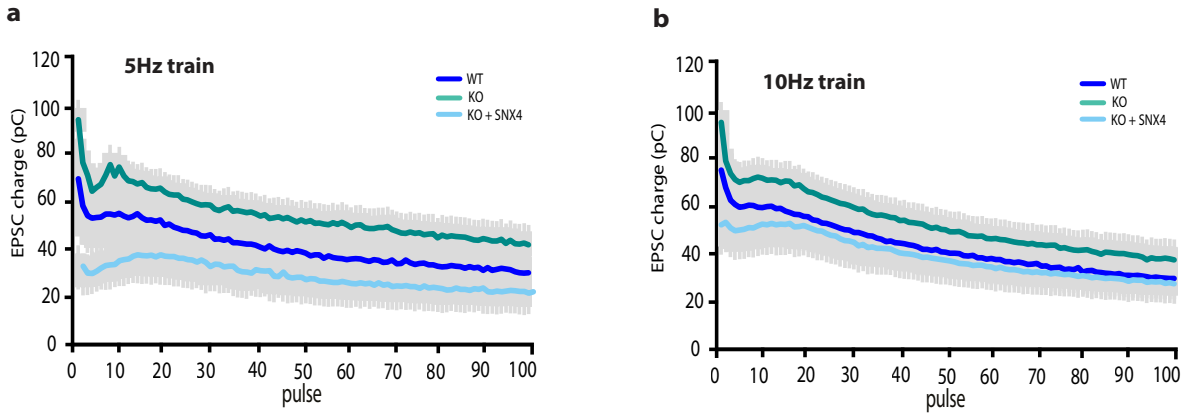

Supplementary figure 2: EPSC charge for 5 Hz and 10 Hz train stimulation.
(a) Mean EPSC charge trace for 100 AP at 5 Hz train. **(b)** Mean EPSC charge trace for 100 AP at 10 Hz train.

Supplementary table 1: Statistics overview

Figure 1	n number (range neurons or synapses per group /animals)	mean	median	SEM	SD	significant test	p-value
snx4 wb	x/3	dcre = 100 21d cre = 9,913 18d cre = 16,87 14d cre = 32,52	dcre = 100 21d cre = 8,489 18d cre = 11,68 14d cre = 19,18	dcre = 0 21d cre = 4,943 18d cre = 9,817 14d cre = 25,52	dcre = 0 21d cre = 8,561 18d cre = 9,817 14d cre = 25,52	Ordinary one way anova	dcre-21d cre = 0,0003 dcre-18d cre = 0,0005 dcre-14d cre = 0,0019
snx4 fluorescence	38-42/6	control = 100,0 KO = 42,66	control = 98,74 KO = 37,46	control = 3,267 KO = 3,471	control = 21,17 KO = 21,40	mann-whitney test	p<0,0001
Dendrite length	32-36/6	control = 1530 KO = 1536	control = 1407 KO = 1389	control = 99,16 KO =109,6	control = 594,9 KO =620,2	mann-whitney test	p = 0,9077
# vamp2 puncta per neuron	35-41/6	control = 605,3 KO = 626,1	control = 536,0 KO =533,0	control = 40,23 KO =61,68	control = 257,6 KO = 364,9	mann-whitney test	p = 0,899
Figure 2							
Amplitude (pA)	25-34/4	control = 6081 KO = 7124 KO + SNX4 = 3508	control = 5272 KO = 6546 KO + SNX4 = 2908	control = 826,1 KO = 1076 KO + SNX4 = 439,6	control = 4817 KO = 5382 KO + SNX4 = 2198	multilevel anova + bonferroni correction	Con-KO = 1 Con-SNX4 = 0,061 KO-SNX4 = 0,0378
Charge (pC)	25-33/4	control = 88,53 KO = 121,7 KO + SNX4 = 57,38	control = 66,98 KO = 78,04 KO + SNX4 = 40,06	control = 15,61 KO = 21,34 KO + SNX4 = 9,295	control = 89,67 KO = 106,7 KO + SNX4 = 47,40	multilevel anova + bonferroni correction	Con-KO = 0,7718 Con-SNX4 = 0,4833 KO-SNX4 = 0,0584
Inter pulse Ratio pulse 25 (p2/p1)	25-33/4	control = 0,9813 KO = 0,8808 KO + SNX4 = 1,022	control = 0,9489 KO = 0,8515 KO + SNX4 = 1,017	control = 0,06983 KO = 0,04791 KO + SNX4 = 0,06540	control = 0,4012 KO = 0,2395 KO + SNX4 = 0,3582	multilevel anova	p = 0,2756
Inter pulse Ratio pulse 50 (p2/p1)	15-19/4	control = 1,088 KO = 0,9564 KO + SNX4 = 1,152	control = 0,9337 KO = 0,9157 KO + SNX4 = 1,138	control = 0,09870 KO = 0,05315 KO + SNX4 = 0,08174	control = 0,3823 KO = 0,2126 KO + SNX4 = 0,3563	multilevel anova	p = 0,198
Inter pulse Ratio pulse 100 (p2/p1)	32-38/4	control = 0,9123 KO = 0,8791 KO + SNX4 = 0,9327	control = 0,8729 KO = 0,8553 KO + SNX4 = 0,9168	control = 0,03475 KO = 0,03696 KO + SNX4 = 0,04336	control = 0,2142 KO = 0,2024 KO + SNX4 = 0,2453	multilevel anova	p = 0,9329
Inter pulse Ratio pulse 200 (p2/p1)	25-29/4	control = 0,8399 KO = 0,8045 KO + SNX4 = 0,8718	control = 0,8257 KO = 0,7830 KO + SNX4 = 0,8747	control = 0,03448 KO = 0,02499 KO + SNX4 = 0,03094	control = 0,1857 KO = 0,1369 KO + SNX4 = 0,1547	multilevel anova	p = 0,3914
Average charge (pulse 90100) (p2/p1)	25-33/4	control = 8,562 KO = 18,15 KO + SNX4 = 9,098	control = 6,557 KO = 9,282 KO + SNX4 = 4,745	control = 1,115 KO = 3,665 KO + SNX4 = 1,545	control = 6,405 KO = 18,33 KO + SNX4 = 8,318	multilevel anova + bonferroni correction	Con-KO = 0,0045 Con-SNX4 = 1 KO-SNX4 = 0,0067
RRP estimate (pC)	25-34/4	control = 783,5 KO = 871,7 KO + SNX4 = 659,3	control = 453,3 KO = 486,1 KO + SNX4 = 581,0	control = 167,2 KO = 158,9 KO + SNX4 = 93,64	control = 975,1 KO = 794,7 KO + SNX4 = 512,9	multilevel anova	p = 0,2124
slope estimate (pC/s)	25-33/4	control = 8,953 KO = 18,67 KO + SNX4 = 9,513	control = 7,074 KO = 9,569 KO + SNX4 = 5,667	control = 1,155 KO = 3,755 KO + SNX4 = 1,589	control = 6,636 KO = 18,78 KO + SNX4 = 8,555	multilevel anova + bonferroni correction	Con-KO = 0,0051 Con-SNX4 = 1 KO-SNX4 = 0,0073
Figure 3							
NH4 intensity	19-21/3	control = 2,053 KO = 1,497	control = 2,005 KO = 1,473	control = 0,1759 KO = 0,1313	control = 0,7668 KO = 0,6018	multilevel anova	p = 0.0152
release fraction first stim	19-21/3	control = 0,1909 KO = 0,2197	control = 0,1880 KO = 0,2031	control = 0,00Ω KO =0,0143	control = 0,0285 KO = 0,0567	multilevel anova	*p = 0.0767*
release fraction 2nd stim	19-21/3	control = 0,1713 KO = 0,2136	control = 0,1772 KO = 0,1850	control = 0,0077 KO = 0,01531	control = 0,0338 KO = 0,0702	multilevel anova	p = 0.018
decay time tau first stim	19-21/3	control = 27,49 KO = 29,85	control = 27,57 KO = 29,59	control = 2,408 KO = 2,553	control = 10,22 KO = 11,42	multilevel anova	p = 0.4929
decay time tau second stim	19-21/3	control = 27,08 KO = 26,16	control = 24,32 KO = 22,23	control = 3,653 KO = 2,517	control = 14,15 KO = 11,54	multilevel anova	p = 0.8255
average active synapses	19-21/3	control = 63,56 KO = 49,49	control = 67,46 KO = 49,70	control = 5,303 KO = 4,130	control =23,12 KO = 19,93	multilevel anova	*p = 0.0691*
FM4-64 release	22-34/4	control = 19,02 KO = 19,24	control = 15,10 KO = 18,56	control = 1,735 KO = 1,635	control = 10,11 KO = 7,667	multilevel anova	p = 0.3109
FM4-64 uptake	22-34/4	control = 100,0 KO = 92,54	control = 99,08 KO = 93,33	control = 3,314 KO = 5,017	control = 19,33 KO = 23,53	multilevel anova	p = 0.3356
Figure 5							
vamp2 puncta per um	35-41/6	control = 0,4829 KO = 0,5289	control = 0,4196 KO = 0,4486	control = 0,02679 KO = 0,03598	control = 0,1715 KO = 0,2128	mann-whitney test	p = 0,5053
vamp2 intensity in neurites	35-41/6	control = 100,0 KO = 92,94	control = 97,53 KO = 86,62	control = 3,505 KO = 5,445	control = 22,44 KO = 33,12	Unpaired t test with Welch's correction	p = 0,28
Figure 6							
fraction docked	174-175/3	control = 4,974 KO = 6,353	control = 4,487 KO = 5,556	control = 0,2251 KO = 0,2992	control = 2,978 KO = 3,946	mann-whitney test	p = 0,0002
# docked normalized to AZ	174-175/3	control = 0,9119377 KO = 1,390216	control = 0,8270241 KO = 1,404846	control = 0,02914 KO = 0,03772	control = 0,3854 KO = 0,4976	mann-whitney test	p < 0,0001
# docked ccv	174-175/3	control = 6,269 KO = 8,190	control = 6 KO = 7	control = 0,3017 KO = 0,3380	control = 3,992 KO = 4,458	mann-whitney test	p < 0,0001
# total ccv	174-175/3	control = 157,2 KO = 160,5	control = 120 KO = 134,5	control = 8,425 KO = 7,726	control = 111,5 KO = 101,9	mann-whitney test	p = 0,3682
vesicle size 0-50	174-175/3	control = 29,34 KO = 28,48	control = 28,50 KO = 27,39	control = 0,1007 KO = 0,1277	control = 8,186 KO = 10,02	multilevel anova	p = <,0001
vesicle size 0-50 per synapse	174-175/3	control = 27,54 KO = 28,48	control = 28,67 KO = 28,02	control = 0,2044 KO = 0,2427	control = 2,727 KO = 3,238	mann-whitney test	p = 0,0007
vesicle size 50 plus per synapse	174-175/3	control = 72,38 KO = 75,89	control = 67,19 KO = 65,95	control = 3,075 KO = 2,991	control = 22,17 KO = 22,18	mann-whitney test	p = 0,3529
vesicle cluster area	174-175/3	control = 0,2193 KO = 0,1741	control = 0,1720 KO = 0,1510	control = 0,01283 KO = 0,008008	control = 0,1697 KO = 0,1056	mann-whitney test	p = 0,0322
actie zone length	174-175/3	control = 706,1 KO = 600,3	control = 617,3 KO = 538,7	control = 29,98 KO = 21,17	control = 396,6 KO = 279,2	mann-whitney test	p = 0,0248
PSD length	174-175/3	control = 701,9 KO = 589,5	control = 611,4 KO = 526,8	control = 30,10 KO = 20,95	control = 398,2 KO = 276,4	mann-whitney test	p = 0,0157